energies

MDPI

Article

Advantage of a Thermoelectric Generator with Hybridization of Segmented Materials and Irregularly Variable Cross-Section Design

Ye-Qi Zhang [1], Jiao Sun [1], Guang-Xu Wang [1] and Tian-Hu Wang [2,3,*]

[1] Department of Mathematics and Physics, North China Electric Power University, Beijing 102206, China; yqzhang@ncepu.edu.cn (Y.-Q.Z.); 120192209805@ncepu.edu.cn (J.S.); 120202209090@ncepu.edu.cn (G.-X.W.)
[2] Key Laboratory of Power Station Energy Transfer Conversion and System, Ministry of Education, North China Electric Power University, Beijing 102206, China
[3] School of Energy Power and Mechanical Engineering, North China Electric Power University, Beijing 102206, China
* Correspondence: thwang@ncepu.edu.cn

Abstract: As a direct energy converter between heat and electricity, thermoelectric generators (TEGs) have potential applications including recovery of waste heat, and solar thermoelectric power generation. Geometric parameter and material are two critical factors to improve the TEG performance. However, the strategies base on structure design and material development are always separated. There are limited studies on the effects of consolidating them simultaneously. Here, an idea of segmented material coupled with irregularly variable cross-section design was conceived to further improve the TEG output power. The performance of TEGs with rectangular leg, segmented leg, variable cross-sectional leg, and the new design are compared. The coupling effects between various mechanisms are revealed, which are responsible for the superior performance provided by the developed design. Based on this knowledge, a multiparameters optimization was performed through the genetic algorithm to reach the optimal combination of design parameters. The results show that, with a constraint of certain material volume, the optimal performance of the TEG can be further enhanced by coupling segmented material and irregularly variable cross-section design. An improvement of 51.71% was achieved when compared with the conventional counterpart. This work offers a simple route to enhance the TEG performance when the device materials are specified, without an increase in the cost of manufacturing.

Keywords: thermoelectric generator; waste heat recovery; segmented material; irregularly variable cross-section; optimization; genetic algorithm

Citation: Zhang, Y.-Q.; Sun, J.; Wang, G.-X.; Wang, T.-H. Advantage of a Thermoelectric Generator with Hybridization of Segmented Materials and Irregularly Variable Cross-Section Design. *Energies* **2022**, *15*, 2944. https://doi.org/10.3390/en15082944

Academic Editors: Amir Pakdel and David Berthebaud

Received: 24 February 2022
Accepted: 13 April 2022
Published: 17 April 2022

1. Introduction

Thermoelectric generators (TEGs) can directly convert heat into electricity by the Seebeck effect [1]. Their compact size, reliability, environmental friendliness, and lack of working fluid and chemical reaction render them a promising candidate for on-chip heat recovery and power generation [2,3]. However, relatively low conversion efficiency and power density fundamentally hinder their applications. It has been experimentally and theoretically demonstrated that the performance is mainly determined by the figure of merit (ZT) of thermoelectric material [4]. Although material development is the most effective way to boost performance, it is challenged that optimizing one physical parameter (e.g., Seebeck coefficient) often deteriorates another (e.g., thermal conductivity) [5]. Thus, the exploration of new thermoelectric materials alone has suffered an efficiency bottleneck. Fortunately, it is demonstrated that architecture optimization is equally important to obtain a better performance [6]. The changed structure causes varied electrical and thermal resistances, influences transport path of the charge carrier, and determines the Joule heat,

Thomson heat, and Fourier heat conduction. Hence, to mediate above multiphysical effects, lots of performance-driven studies involving architecture design of TEG have been performed [7–20].

One effective way is introducing variable cross-section (VCS) geometry of the legs. There are elaborately designed TEGs including diverse leg shapes and different structures, significantly improving the performance. However, the contributions mainly focused on regular cross-section, including exponential-shaped leg [7], frustum-shaped leg [8], tapered leg [9], T-shaped configuration [10], X-leg [11], etc. [12–14]. Due to the limitation of regular function shape, the cross-section cannot change freely so that it is unable to reach maximum performance. Thus, there is a strong need to perform a constraint-free irregularly variable cross-section design (IVCS). Unfortunately, the relative studies are very limited. In addition to geometric factors, segmented design is also critical [15,16]. During a TEG operation, a temperature gradient is established across the leg from the heat source to the heat rejection end. Most materials cannot hold the best performance if they are not in their work temperature regime. As a function of temperature, *ZT* varies over the length of the device, causing TEGs to lose efficiency [4,17,18]. Hence, it is essential to examine the performance considering both the material and device parameters. In recent years, researchers found that segmental or functionally graded material enable striking improvement of the output power [19–25]. The core design strategy consists in making the divided material operate in its most suitable temperature regime. However, most of the pertinent designs only involve segmented idea but overlook the variable cross-section effects.

It can be concluded that although significant progress has been made to boost TEG performance, there has been no report on combining segmented and irregularly variable cross-section (S-IVCS) design together. The potential contributions in this work could be summarized as: (1) In the previous studies, variable cross-sections improved performance. Segmented design can also boost performance. It is expected that hybridization of thermoelectric segmented material and irregularly variable cross-sectional structures may enable synergistic advantages (see Figure 1b). (2) Neither segmented nor irregularly variable cross-section, the influential factors are diversely variable (e.g., geometric parameters, material, external load). There will be strong coupling phenomena to be explored for S-IVCS design. The feasibility and mechanism to further improve performance are unknown and deserve exploration. (3) The parameter combination corresponding to the optimal performance and the design strategy remain unsolved. Optimizing the structure is a promising way to enhance the TEG performance without an increase in the cost of manufacturing.

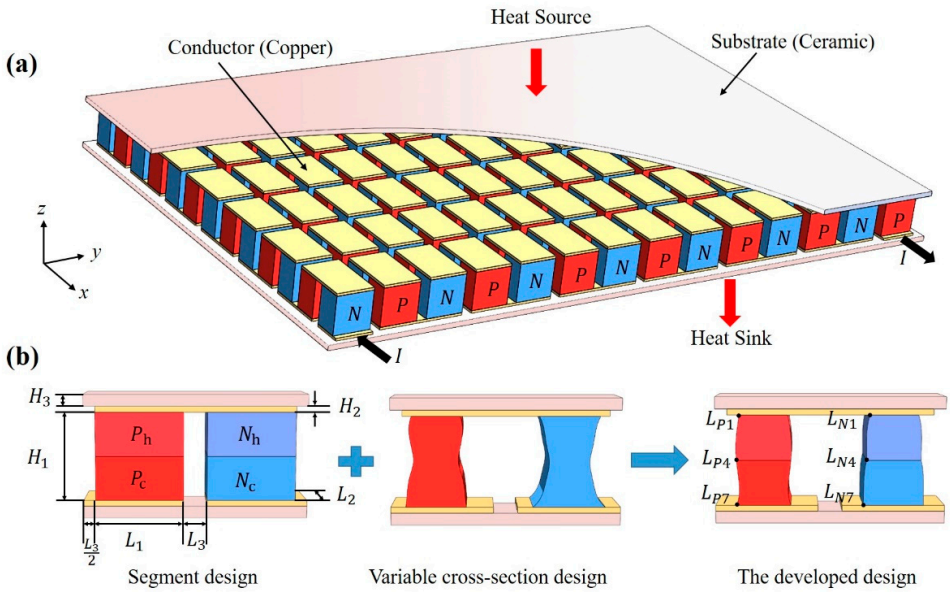

Figure 1. (**a**) Schematic diagram of the thermoelectric module and (**b**) Structure of the unit and the new design concept.

Based on the above analysis, this work aims to justify the feasibility and reveal the mechanism of S-IVCS design strategy. The remainder of the paper is organized as follows. Firstly, a multiphysical TEG model is introduced and the feasibility of S-IVCS design to further improve performance is justified. Then, a multiparameters genetic algorithm is coupled into the model to find the optimal design considering segment material and irregular geometry simultaneously. Finally, the underlying physics behind the improvement is elucidated.

2. Physical Model

2.1. TEG Structure Design

As shown in Figure 1a, a TEG module is composed of dozens of thermocouples, which are connected electrically in series and thermally in parallel. As one unit of the module, each thermocouple consists of a P-type and an N-type semiconductor leg, which are connected by thin metal connectors and sandwiched between two ceramic insulated plates. During power generation, the heat is absorbed from the top ceramic plate, transferred across the thermocouples, and removed by the heat sink at the bottom. Considering the periodic feature of the module, only one unit was simulated in this study. Figure 1b plots the structure of the unit, of which the geometric parameters are listed in Table 1.

Table 1. Geometric parameters of the thermoelectric unit.

L_1	L_2	L_3	H_1	H_2	H_3
1.5 mm	1.0 mm	0.4 mm	3.0 mm	0.1 mm	0.2 mm

Due to their better performance at relative high temperature, $Ce_{0.9}Fe_3CoSb_{12}$ and $Yb_{0.35}Co_4Sb_{12}$ are selected as the P- and the N-type semiconductor material, respectively, for the hot side segment, while $Bi_{2-x}Sb_xTe_3$ (P-type) and $Bi_2Te_{3-x}Se_x$ (N-type) are used for the cold side segment because they are advantageous in low temperature regime. The temperature-dependent properties of the materials are detailed in Ref. [18]. The thermal conductivity, density, and specific heat capacity of the copper connectors are $\lambda_{Cu} = 400\ \mathrm{W/(mK)}$, $\rho_{Cu} = 8960\ \mathrm{kg/m}$, and $C_{p,Cu} = 385\ \mathrm{J/(kg\ K)}$, respectively. The thermal conductivity, density, and specific heat capacity of the ceramic plates are $\lambda_{Cer} = 175\ \mathrm{W/(mK)}$, $\rho_{Cer} = 178,00\ \mathrm{kg/m}$, and $C_{p,Cer} = 132\ \mathrm{J/(kg\ K)}$, respectively.

2.2. Governing Equations

The Fourier heat conduction, Joule heating, Thomson effect, and Peltier effect are multiphysically coupled with each other in the model. When the TE unit operates in steady-state mode, the governing equations read as follows.

Energy conversion equation

$$\nabla \cdot \boldsymbol{q} = Q \tag{1}$$

Current continuity equation

$$\nabla \cdot \boldsymbol{j} = 0 \tag{2}$$

where $\boldsymbol{q}$, Q, and $\boldsymbol{j}$ are the heat flux, the Joule heat, and the current density vector, respectively, which can be further coupled by the following thermoelectric equation as

$$\boldsymbol{q} = -\lambda \nabla T + \alpha T \boldsymbol{j} \tag{3}$$

$$Q = -\nabla U \cdot \boldsymbol{j} \tag{4}$$

$$\boldsymbol{j} = -\sigma(\nabla U + \alpha \nabla T) \tag{5}$$

where λ is the thermal conductivity, α is the Seebeck coefficient, σ is the electric conductivity, T is the temperature, and U is the electric potential.

Based on Equations (2)–(5), the energy conversion equation can be rewritten as

$$\nabla \cdot (\lambda \nabla T) + \boldsymbol{j} \cdot \frac{\boldsymbol{j}}{\sigma} - T \nabla \alpha \cdot \boldsymbol{j} = 0 \quad (6)$$

where the first term is Fourier heat conduction, the second term is Joule heat, and the third term is Peltier effect ($\nabla \alpha$ at the junction) and Thomson effect ($\nabla \alpha$ in thermal gradient).

2.3. Irregularly Variable Cross-Section Design and Boundary Conditions

Considering that the material properties of the P-leg and the N-leg distinctly vary with temperature, their optimal designs may be significantly different. Therefore, the P-leg and N-leg are both optimized. As shown in Figure 1b, for each leg, seven anchor points with uniform distribution along the leg height and with variable locations in the width are designed to control the irregularly variable cross-sectional area. Here, the variable anchor points are P_1, P_2, P_3, P_4, P_5, P_6, and P_7 for the P-leg and N_1, N_2, N_3, N_4, N_5, N_6, and N_7 for the N-leg. The above anchor points are search-variables during the optimization. The consequent leg geometry can be constructed by an interpolation curve of the anchor points. In this case, all variable cross-sections will be rectangular-shaped in the *x*-*y* plane, where the seven side lengths (L_{Pi}) for P-leg and seven side lengths (L_{Ni}) for N-leg are varied. The dimensionless parameters γ (ratio of the hot side height of the P-leg to the total height H_1) and δ (ratio of the hot side height of the N-leg to the total height H_1) are used to control the segmented material of the thermoelectric leg. In addition, the applied current, I, is also regarded as one of the optimization variables. For the thermal boundary conditions, the top surface of the TEG is set as $Q = 0.5$ W, while the bottom surface is fixed as $T_c = 300$ K. Other surfaces are defined as thermally insulated. For the electric conditions, the N-leg end is injected with a current of I, indicating the corresponding resistance load. The P-type end is set as ground.

2.4. Optimization Algorithm

In terms of the S-IVCS performance, the interplay between various influential parameters are complex. It is consequently hard to find the optimal parameter combination without a multiparameters optimization. There are several algorithms to perform the optimization, such as Particle Swarm Optimization (PSO), Differential Evolution (DE), and Genetic Algorithm (GA). PSO could operate without any specific knowledge about the problem, but it often fails in searching the global optimal solution when the objective function has a large number of dimensions [26]. DE is a simple and efficient technique for solving global optimization problems. However, DE may occasionally suffer from problems of stagnation or losing its diversity [27]. GA is popularly used in various optimization problems in science and engineering. It can widely handle complex optimization with nonlinear or non-stationary fitness functions even with random noise [28]. In the open literature, GA is suitable and commonly used for optimization of thermoelectric devices [29,30]. Thus, GA is adopted in this paper.

Figure 2 plots the flow chart of the optimization procedure. The finite element method is employed to solve the direct problem, and a single-objective GA is coupled into the above model to optimize the output power. During optimization, GA operates through four steps involving population initialization, selection, crossover, and mutation. Following the above steps, a population is generated, and the iteration continues until the convergence condition is achieved. It is worth indicating that in the entire optimization process, the crossover and mutation probabilities are set as 0.9 and 0.2, respectively. The population size and the evolutionary generation number are 30 and 200, respectively. The ranges of the search-variables in the model are defined as

$$0.1 < L_{Pi} < 0.5\ (i = 1, 2, \ldots, 7)$$
$$2 < L_{Ni} < 2.4\ (i = 1, 2, \ldots, 7)$$
$$0.3 < \gamma < 0.8$$
$$0.3 < \delta < 0.8$$
$$0.1 < I < 2.0$$

To achieve the maximum output power P_{max}, the fitness function, F_{fit}, is defined as

$$F_{\text{fit}} = \frac{1}{P+1} = \frac{1}{U \times I + 1} \tag{7}$$

where P is the output power and I is the electric current.

In the optimization process, it should be noticed that the temperature may be higher than the suitable working temperature range of the material during the constantly changing geometry and boundary conditions. To avoid this problem, four judgment functions (T_{Ph} < 800 K, T_{Nh} < 800 K, T_{Pc} < 550 K, and T_{Nc} < 500 K, which denote maximum temperature of the hot segment of P-leg, hot segment of N-leg, cold segment of P-leg, and cold segment of N-leg, respectively) are employed to ensure that the four kinds of thermoelectric materials operate in their suitable temperature regimes.

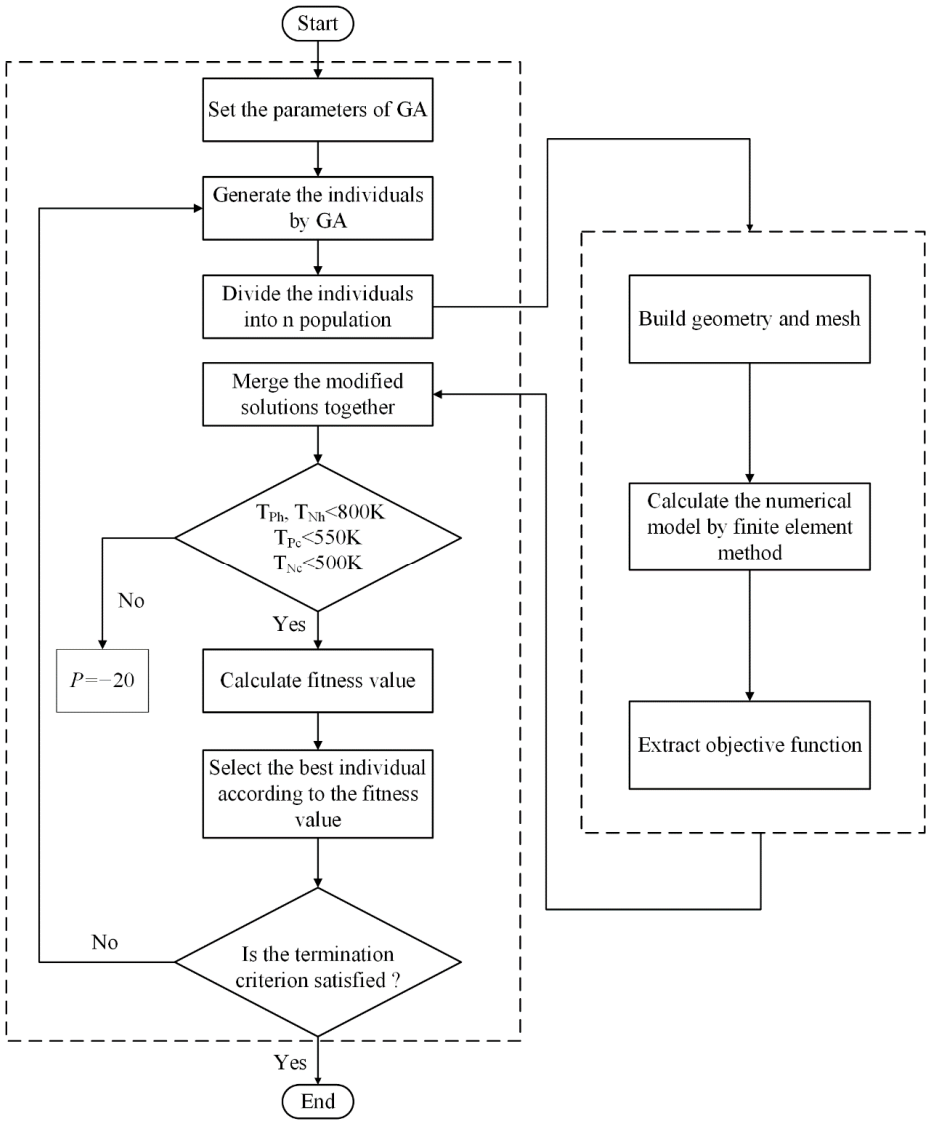

Figure 2. Flow chart of the optimization.

2.5. Model Validation

Before simulation, the grid independence test was examined to ensure the accuracy of the results. To validate the model, the experimental results from three research groups of Hu et al. [31], Hsu et al. [32], and Shen et al. [33] are compared with the present model, respectively. In Hu et al.'s study, the TEG is composed of a single N-type Bi_2Te_3 leg and copper connectors. Two cases with different leg heights are compared with the present model. The size of case 1 is 2.98 × 2.215 × 6.22 mm^3, and case 2 is 2.98 × 2.215 × 9.68 mm^3. The boundary conditions are set as the same with those in Ref. [31] (i.e., 420.75 K for the hot end and 296.55 K for the cold end). The compared results for the *I-U* curve are shown in Figure 3a, demonstrating a reasonable agreement with a maximum error < 5%. In the report of Hsu et al. [32], a TEG module consisting of 199 pairs of TE legs was performed. The TEG measurement system is composed of the heater, copper plate, TEG module, and liquid cooling system. Each TE leg has dimensions of 2 × 2 × 0.64 mm^3. Here, we consider two cases with different thermal boundary conditions for comparison. In case 1, the cold and hot side temperatures are set as 318.788 K and 330 K. In case 2, the cold and hot side temperatures are 304.992 K and 320 K. It should be indicated that the additional thermal and electrical resistance are modeled in the present simulation by the method given in Ref. [34]. Figure 3b shows the characteristics of the *I-U* curves of the present model compared with the experiments of Hsu et al., giving evidence that a good agreement can be observed. The model was also validated by Shen et al.'s experiment, where a commercial thermoelectric cooler with traditional TE element was tested [33]. The design parameters and material properties are identical to those listed in Table 1 in Ref. [33]. The boundary conditions are the same with the experiment. As shown in Figure 3c, the calculated temperature of the hot side agrees well with the experiment data, which further validates the model.

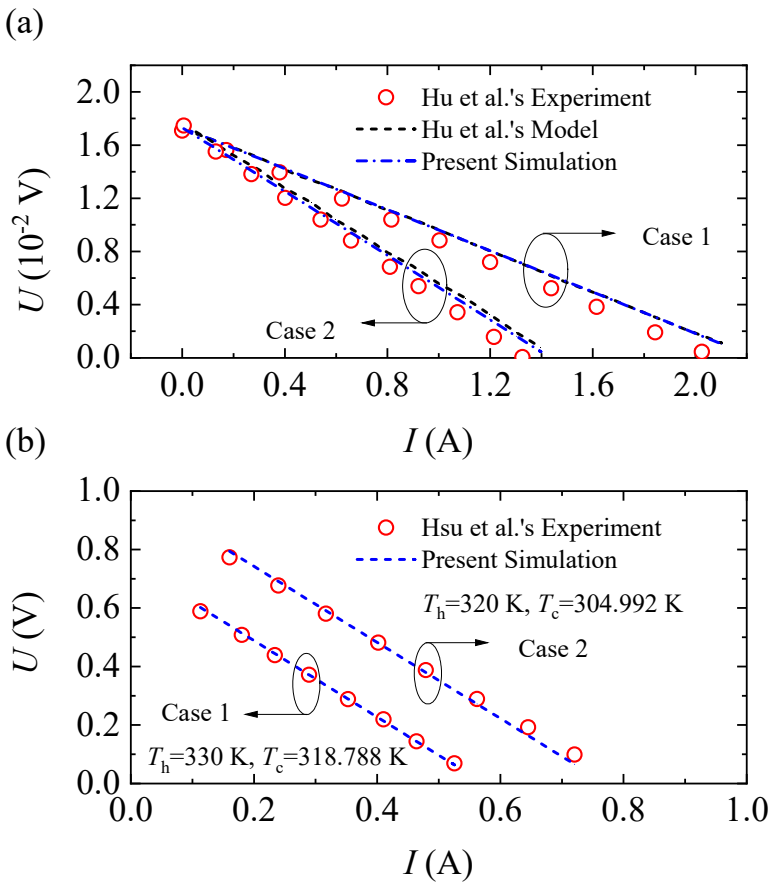

Figure 3. *Cont.*

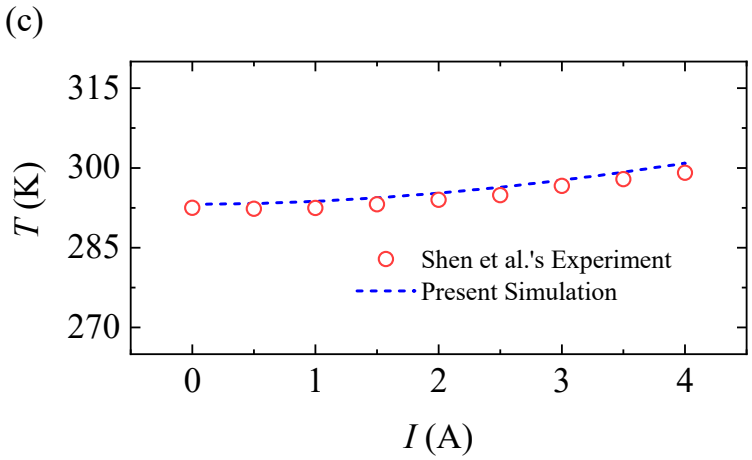

Figure 3. Model validation: (**a**) *I-U* relationship compared with Ref. [31]; (**b**) *I-U* relationship compared with Ref. [32]; (**c**) Temperature of the hot side end compared with Ref. [33].

3. Results and Discussion

3.1. Effects of Segment Material Coupled with Irregularly Variable Cross-Section

In this section, performances of the TEGs with only segment material, only IVCS, and S-IVCS design will be comparatively examined. As shown in Figure 4, the output power as a function of current for segmented designs is compared with the structure with uniform material. Here, four combinations of γ and δ are specified to determine different segmented structure (i.e., γ = 0.4 and δ = 0.9; γ = 0.4 and δ = 0.6; γ = 0.8 and δ = 0.6; γ = 0.8 and δ = 0.9). As a reference structure, the conventional TEG with uniform material is also designed for comparison, in which the P- and the N-leg volume keep the same with the segmented design. It is demonstrated that the segmented design can significantly improve the performance, which is consistent with the previous studies. The max power is below 30 mW for the uniform design, surpassed by all the cases of segmented ones. Additionally, the working regime is also extended to a larger one. The reason is that the temperature follows into the appropriate regime for each segment to preserve a suitable *ZT* value. However, the performance is significantly susceptible to the segment configuration. The combination of γ = 0.4 and δ = 0.6 exhibits the highest power, while the case of γ = 0.8 and δ = 0.9 presents the lowest. The temperature profile and the appropriate segmented pattern are mutually influenced. This justifies the necessity to optimize the parameters of γ and δ to find an optimal segment structure.

As shown in Figure 5, the output power varied with current for different IVCS designs is compared with the rectangular structure. Three pairs with different material volumes (each pair contains an IVCS and a rectangular design with the same volume) are compared. In Pair 1, the volume is 3.00 mm^3 for the P-leg and 2.82 mm^3 for N-leg; In Pair 2, the volume is 3.17 mm^3 for the P-leg and 2.98 mm^3 for the N-leg; In Pair 3, the volume is 3.08 mm^3 for the P-leg and 2.45 mm^3 for the N-leg. The corresponding design parameters determining the cross-section patterns of the designs are listed in Table 2. It is found that the IVCS design is superior to the rectangular one for each pair. The performances are also distinct for different volumes with the cross-sectional areas very different. Thus, a particular cross-sectional area significantly influences the output power. To design an optimal cross-section pattern with a certain material volume remains unknown. Consequently, finding out the most suitable cross-section pattern is another critical issue.

Based on the above analysis, the coupling of IVCS and segmented material together is expected to further improve the performance. As shown in Figure 6, the only IVCS design presents the lowest *I-P* performance. The segmented design holds a larger power and an expanded working regime, and it also presents a more appreciable influence on the performance than IVCS. However, neither of these two designs enables optimal performance. When simultaneously considering the segment and the IVCS (i.e., the S-IVCS

design), the performance can be further improved. However, not all the S-IVCS cases are superior to the separated designs, which is significantly dependent on the cross-sectional pattern. As evidenced in Figure 6, the performance of S-IVCS 1 outperforms the segmented design, while S-IVCS 2 presents a degraded performance. It can be concluded that, although the idea of S-IVCS has the potential to further improve the performance, the appropriate design is unknown and sometimes it can also deteriorate the power. Accordingly, an optimization of IVCS coupled with the segment design is necessary.

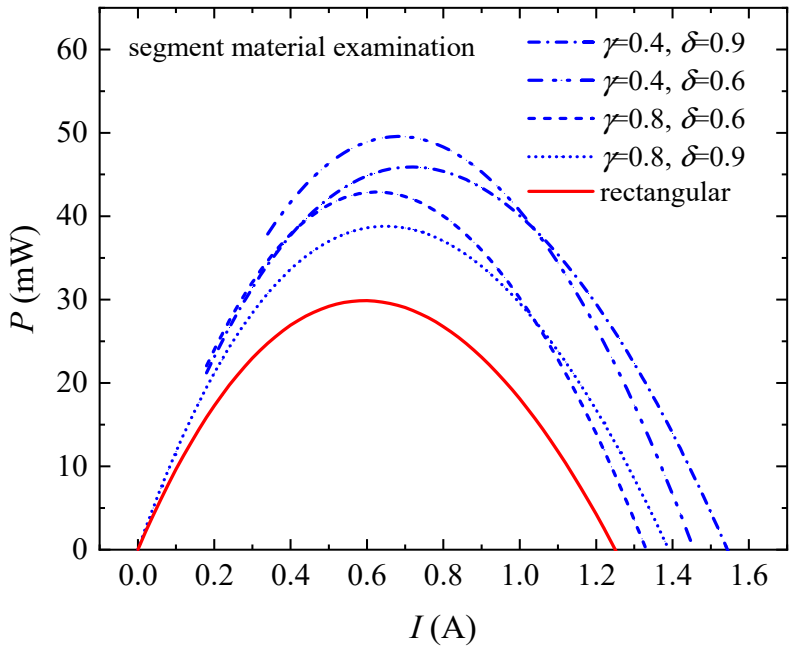

Figure 4. Unit power as a function of current with various segmented designs compared with the uniform material structure.

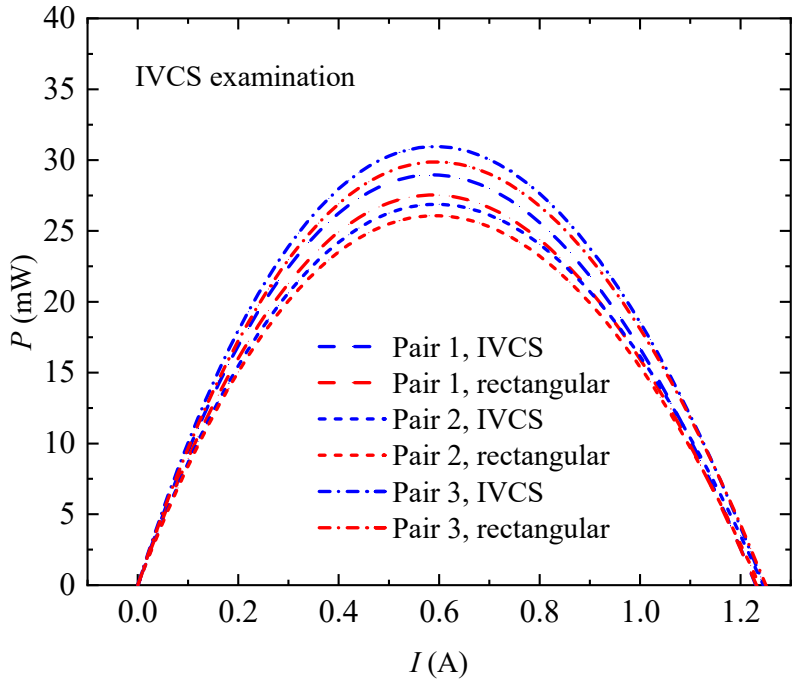

Figure 5. Unit power as a function of current with various cross-sectional designs compared with the rectangular structure.

Table 2. Design parameters of the three IVCS patterns shown in Figure 5.

	Volume (mm^3)	Design	P_1 (mm)	P_2 (mm)	P_3 (mm)	P_4 (mm)	P_5 (mm)	P_6 (mm)	P_7 (mm)
P-leg	3.00	IVCS 1	0.40	0.35	0.30	0.25	0.20	0.15	0.10
		Rect.	0.25	0.25	0.25	0.25	0.25	0.25	0.25
	3.17	IVCS 2	0.35	0.25	0.15	0.05	0.15	0.25	0.35
		Rect.	0.22	0.22	0.22	0.22	0.22	0.22	0.22
	3.08	IVCS 3	0.30	0.35	0.30	0.25	0.20	0.10	0.15
		Rect.	0.24	0.24	0.24	0.24	0.24	0.24	0.24
	Volume (mm^3)	design	N_1 (mm)	N_2 (mm)	N_3 (mm)	N_4 (mm)	N_5 (mm)	N_6 (mm)	N_7 (mm)
N-leg	2.82	IVCS 1	2.00	2.05	2.10	2.20	2.25	2.30	2.35
		Rect.	2.18	2.18	2.18	2.18	2.18	2.18	2.18
	2.98	IVCS 2	2.00	2.10	2.20	2.30	2.20	2.10	2.00
		Rect.	2.15	2.15	2.15	2.15	2.15	2.15	2.15
	2.45	IVCS 3	2.30	2.10	2.20	2.30	2.25	2.30	2.35
		Rect.	2.24	2.24	2.24	2.24	2.24	2.24	2.24

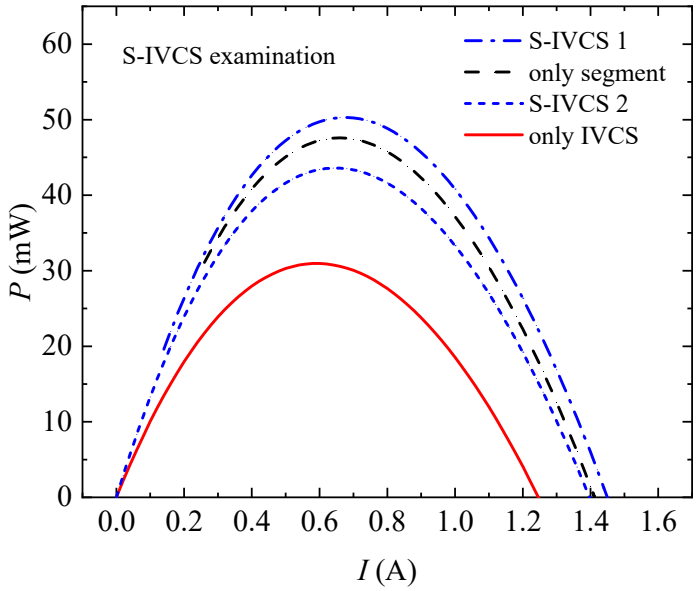

Figure 6. Comparison of the unit power as a function of current with various designs of only segmented, only IVCS, S-IVCS 1, and S-IVCS 2. Here, the material volume of the different designs keeps the same.

Two factors are essential for performance improvement. One is the segment pattern and the other one is the leg shape, which are mutually coupled under different conditions. The improved performance of the new design can be demonstrated through the temperature distribution shown in Figure 7. Here, the temperature contours for I = 0.6 and I = 1.2 A are plotted. Both the modified cross-section and re-allocated material volume along the leg length change the Seebeck effect and Fourier heat conduction, leading to a more suitable temperature profile. It is evidenced that S-IVCS 1 exhibits the largest temperature gradient, followed by the only-segmented, and then S-IVCS 2. The only IVCS design presents the smallest temperature gradient. A larger temperature difference enables a better output power. This justifies the necessary optimization of the whole device both considering the segmented and the irregularly variable cross-sectional parameters. According to the above analysis, multiparameters optimization is necessary to achieve better performance.

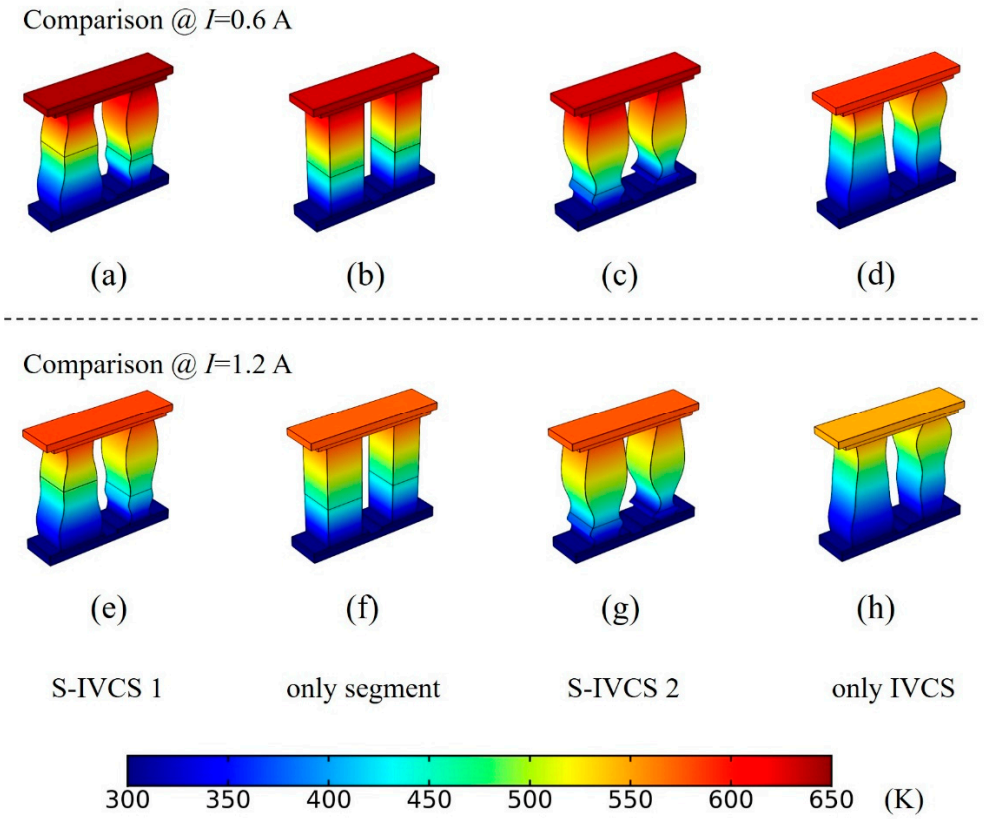

Figure 7. Temperature distribution of the four different designs at different current: (**a**–**d**) at current of 0.6 A; (**e**–**f**) at current of 1.2 A.

3.2. Optimization of the S-IVCS Design

A genetic algorithm described in Section 2.4 is employed to perform the optimization. The cases of IVCS and S-IVCS are both optimized for comparison. Tables 3 and 4 list the design parameters (P_1–P_7 for P-leg and N_1–N_7 for N-leg) as well as the operational parameters (I, γ, and δ) for the two optimized structures. As shown in Figure 8, the output power as a function of generation number during optimization is presented. The design of IVCS shows modest improvement in output power (from 33.34 to 41.48 mW), which is outperformed by the S-IVCS design (from 48.50 to 59.90 mW). It is evidenced that only using variable cross-section has its limitation in power boosting. However, when segmented and irregularly variable cross-section are both considered, the power can be further significantly enhanced.

Table 3. The design parameters of the S-IVCS optimization.

P_1 (mm)	P_2 (mm)	P_3 (mm)	P_4 (mm)	P_5 (mm)	P_6 (mm)	P_7 (mm)
0.41	0.48	0.49	0.26	0.44	0.23	0.31
N_1 (mm)	N_2 (mm)	N_3 (mm)	N_4 (mm)	N_5 (mm)	N_6 (mm)	N_7 (mm)
2.27	2.32	2.39	2.40	2.28	2.40	2.29
I (A)	γ	δ	P_{opt} (mW)	P_{rect} (mW)		
0.66	0.56	0.76	59.91	39.49		

Table 4. The design parameters of the IVCS optimization.

P_1 (mm)	P_2 (mm)	P_3 (mm)	P_4 (mm)	P_5 (mm)	P_6 (mm)	P_7 (mm)
0.14	0.27	0.50	0.49	0.44	0.27	0.14
N_1 (mm)	N_2 (mm)	N_3 (mm)	N_4 (mm)	N_5 (mm)	N_6 (mm)	N_7 (mm)
2.40	2.29	2.40	2.40	2.37	2.40	2.13
I (A)	P_{opt} (mW)	P_{rect} (mW)				
0.48	41.48	38.56				

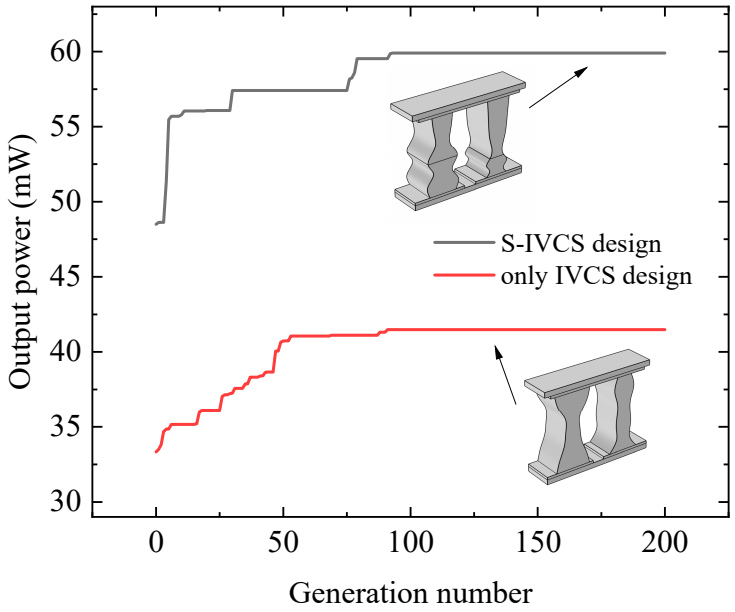

Figure 8. The output power as a function of generation number during the optimization.

The corresponding optimized structures are shown in Figure 9. The IVCS and the S-IVCS design are compared with their rectangular counterparts with the same volume, respectively (For the IVCS design, the volume is 2.38 mm^3 for the P-leg and 1.75 mm^3 for the N-leg. For the S-IVCS design, the volume is 2.21 mm^3 for the P-leg and 1.75 mm^3 for the N-leg). It is evidenced that the materials are re-distributed along the leg length. The shape of the P-leg is different from the N-type one. The segmented pattern of the P-type is also distinct from the N-type one. Compared with their rectangular ones, the output power increases from 38.56 to 41.48 mW for the IVCS, and from 39.49 mW to 59.91 mW for the S-IVCS. The betterments are enhanced by 7.57% and 51.71%, respectively. This result evidently verifies the superiority of the S-IVCS design concept.

Furthermore, the *I-P* curves for the two optimized designs are shown in Figure 10. It is found that the performances are improved for both the two designs compared with their rectangular counterparts. In particular, the S-IVCS improves the power sharply than the only IVCS design. Moreover, the optimized current is larger for S-IVCS than IVCS. This optimal value is around 0.65 A, almost the same as that obtained by GA, justifying the accuracy of the optimization results. The consequential working regime also expands from 1.18 to 1.32 A. Once again, it justifies that the best output power cannot be achieved only by shape optimization, but can be realized by S-IVCS design concept. It is easy to understand that material property is critical to boost performance. The material profile along the leg is distinctly different for the two designs, which causes different thermal and electrical resistances. The resultant modification of Joule heat and electric potential contribute the improved performance. The underlying physics will be illustrated in Section 3.3.

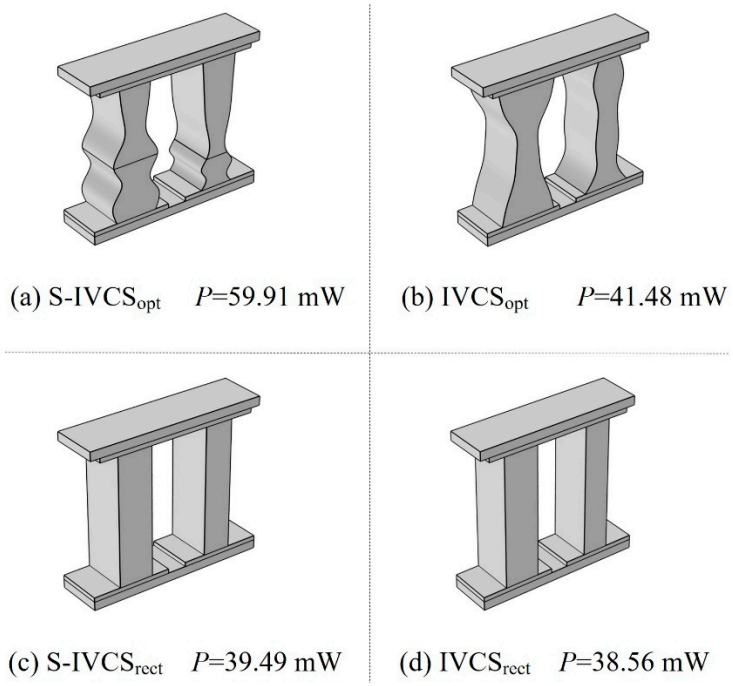

Figure 9. The optimized designs compared with the conventional ones with the same volume. (**a**) S-IVCS; (**b**) IVCS; (**c**) rectangular counterpart of S-IVCS; (**d**) rectangular counterpart of IVCS.

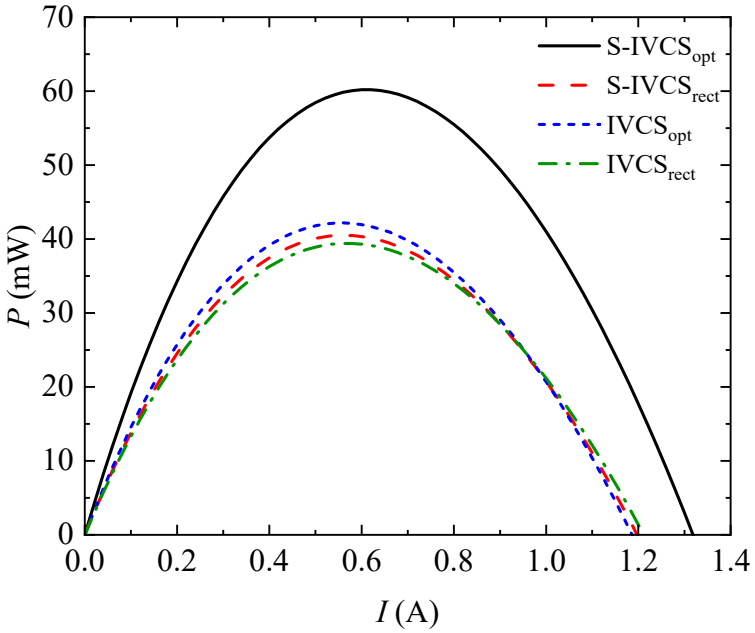

Figure 10. Comparison of the *I-P* curves for the four designs.

Thermal boundary conditions will influence the optimized performance. Besides T_c = 300 K, the optimizations of IVCS and S-IVCS are also performed at other T_c. The optimized structures for S-IVCS and IVCS at T_c = 280 K, 300 K, and 320 K are shown in Figure 11. The corresponding output powers are plotted in Figure 12. For comparison, the output power of rectangular shape designs (with the same volume to each optimized structure) are also shown. The optimized structure changes significantly for different T_c. For each T_c, the new design S-IVCS$_{opt}$ holds the best performance, sharply outperforming other designs. Compared with the rectangular counterparts, the improved degree for the S-IVCS is strikingly higher than the IVCS, further indicating the advantage of the proposed

design. At T_c = 300 K, in particular, the material volume needed for S-IVCS$_{opt}$ (3.96 mm^3) is smaller than that for IVCS$_{opt}$ (4.13 mm^3). It can be also found that, at higher T_c, the optimal output power is decreased caused by the smaller temperature difference across the device.

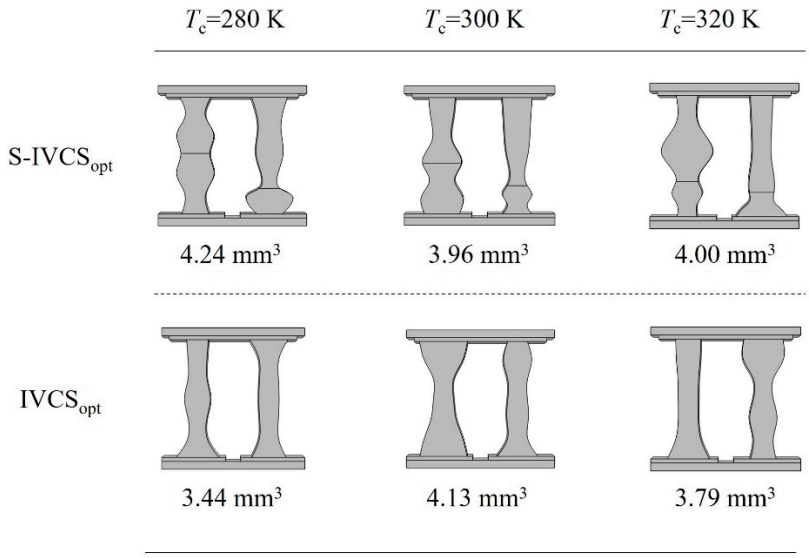

Figure 11. The optimized structures for S-IVCS and IVCS at T_c =280 K, 300 K, and 320 K.

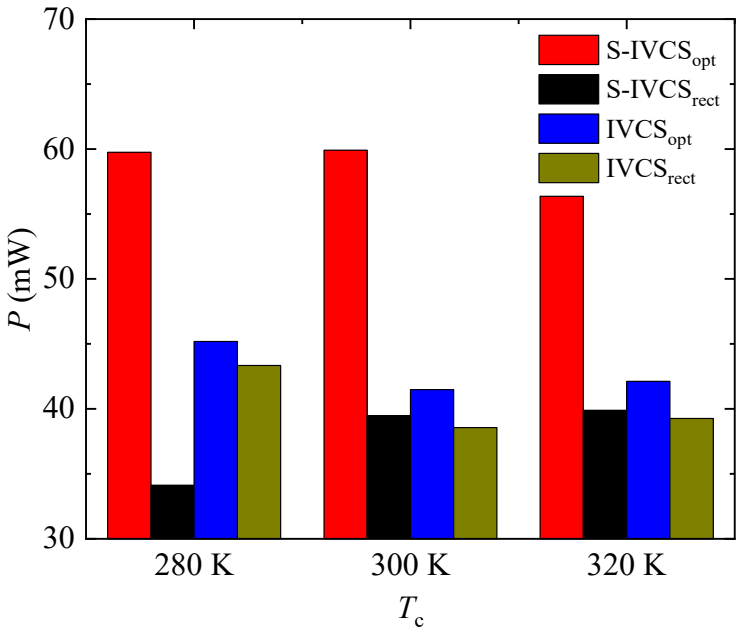

Figure 12. Comparison of the output power for various designs at T_c = 280 K, 300 K, and 320 K.

3.3. Physics behind the Advantageous Performance

How does the integration of segmented material with irregularly variable cross-section strengthen power generation? The temperature and electric potential fields are mutually coupled with each other. The segmented design renders the materials suitable for the right temperature regime, and also influences the temperature and potential distribution. The thermal and electrical resistances are significantly influenced by the geometry, which resultantly causes the changed Peltier heat, Joule heat, and thermal conduction. It is a strong coupling phenomenon and it is not easy to clarify the effect of a particular factor. The optimized topography not only renders the thermal resistance re-distributed but also alters the electrical resistance profile, which results in the best temperature and potential

distributions. Figure 13 shows the temperature and potential distributions through the leg to provide evidences for the above judgment.

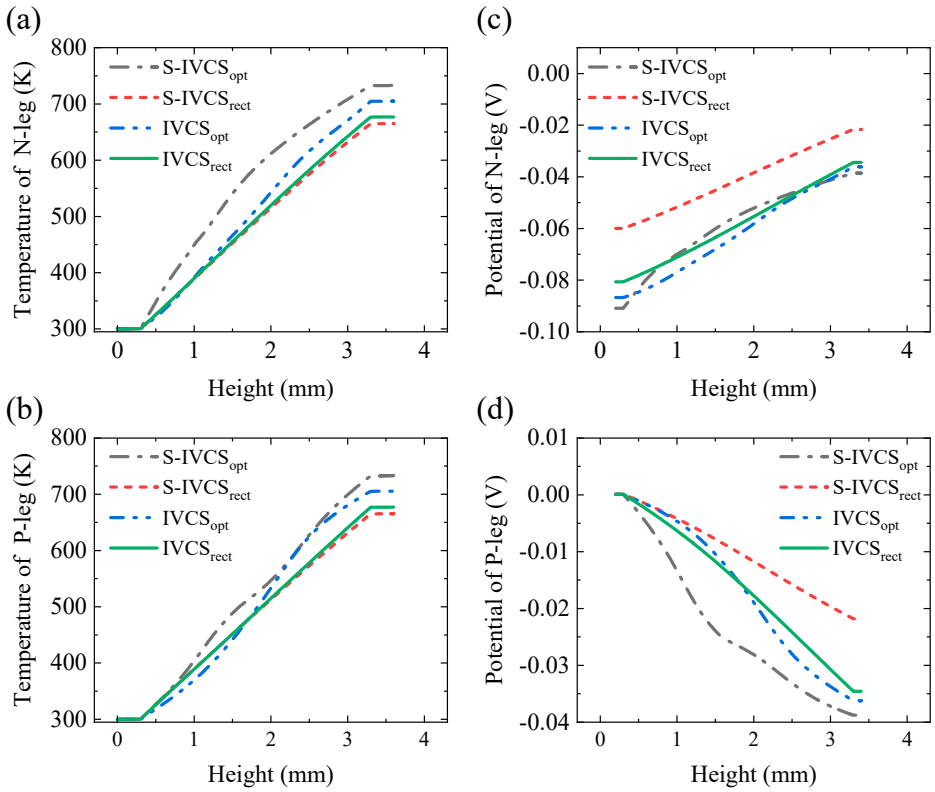

Figure 13. Temperature and electric potential distribution comparison between the four designs: (**a**) temperature of N-leg; (**b**) temperature of P-leg; (**c**) potential of N-leg; (**d**) potential of P-leg.

The following items will change during the optimization procedure: (1) There is a temperature gradient along the leg length. γ and δ are changed to allocate suitable volume to each material according to the temperature regime. (2) A larger cross-section area means a larger volume. The changed cross-section area at different heights also contributes to volume distribution. At a suitable temperature regime, more material should be allocated. (3) When the above two factors are optimized, the thermal and electrical resistances are updated. Because a TEG has a working curve of output power versus applied current, the current also changes to meet the suitable resistance. Remember that the top surface of the TEG unit is fixed as $Q = 0.5$ W and the bottom surface is set as $T_c = 300$ K. Thus the changed thermal resistance will alter the temperature profile along the leg length.

Figure 13a,b show the temperature of the optimized S-IVCS and IVCS designs compared with their rectangular counterparts, respectively. Here, Figure 13a for the N-leg and Figure 13b for the P-leg. It is apparent that the optimized structures hold a higher temperature and a larger temperature difference. For the conventional designs, the two temperature profiles keep almost the same. After optimization, both two designs elevate the temperature. The temperature also changes from a linear to a curved one caused by the irregularly changed shape. For the optimized P-leg, the temperature is lower at the bottom segment and higher at the upper segment. However, the increase degree of temperature in the S-IVCS presents a higher rate than the IVCS. The temperature becomes higher across the whole leg by the optimization of S-IVCS. The reason is that the low-temperature material occupies a larger leg volume. To compensate the performance of the high-temperature material, the algorithm needs to elevate the temperature.

Figure 13c,d show the electric potential for the two optimized designs compared with the rectangular ones. It is found that the potential changes slightly after optimization for the IVCS design, but changes strikingly for the S-IVCS design. The reason may be attributed

to the different materials with the distinct property of electrical and thermal resistances, which strongly changes the internal resistance. This is consistent with the results reported by Ge et al. [35], where it is demonstrated that variable cross-section may cause internal resistance variation. The corresponding temperature and potential contours are shown in Figures 14 and 15, respectively. It shows that the temperature and the potential change significantly after optimization.

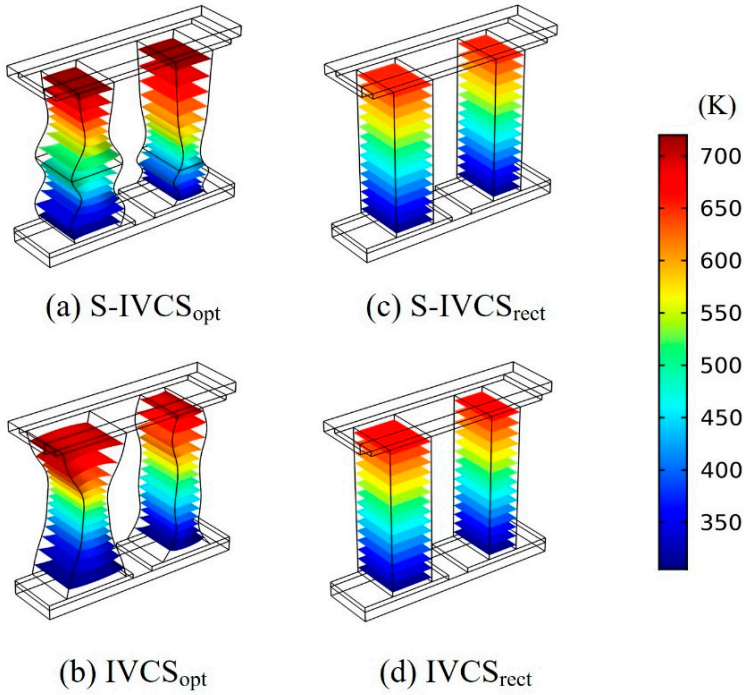

Figure 14. Temperature contour comparison between the four designs.

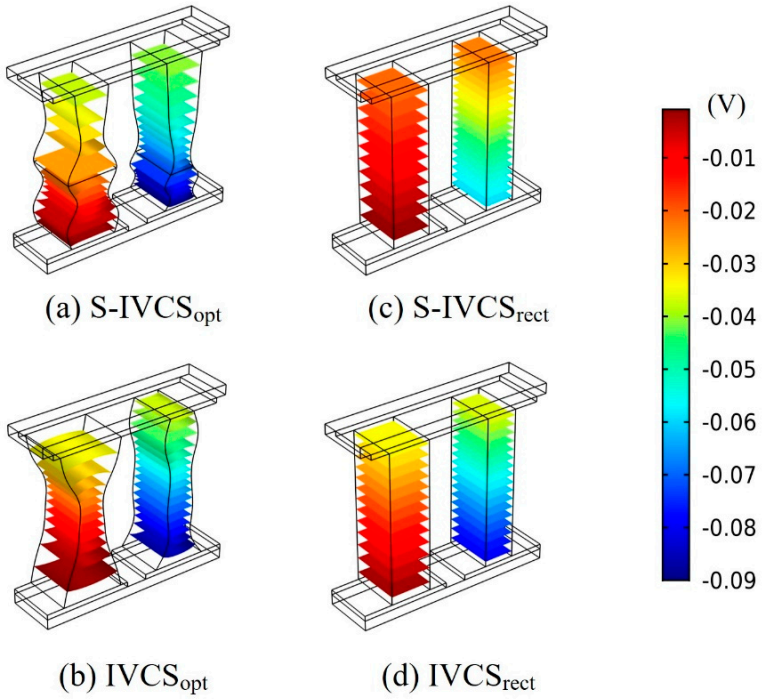

Figure 15. Electric potential contour comparison between the four designs.

Additionally, the average figure of merit of the optimized S-IVCS$_{opt}$ are compared with others to evidence the superior performance, which is calculated as

$$M = \frac{1}{V}\int_0^H ZTAdh \tag{8}$$

where V is the leg volume, H is the leg height, ZT is the figure of merit as a function of h, and A is the cross-sectional area as a function of h. The value of M for each leg is shown in Table 5. It is confirmed that either for the P-leg or the N-leg, the proposed design holds the highest M.

Table 5. The average figure of merit of the four designs.

	Designs	Average Figure of Merit $\overline{ZT}$
P-leg	S-IVCS$_{opt}$	0.86575
	S-IVCS$_{rect}$	0.53359
	IVCS$_{opt}$	0.50990
	IVCS$_{rect}$	0.52500
N-leg	S-IVCS$_{opt}$	1.05570
	S-IVCS$_{rect}$	0.87312
	IVCS$_{opt}$	0.87913
	IVCS$_{rect}$	0.86025

The S-IVCS$_{opt}$ design is also compared with other studies. Ibeagwu [36] compared TEG geometries such as trap-leg, Y-leg, and X-leg. It is found that the X-leg generates about 19.13% more power than the convectional geometry. Al-Merbati [37] propsed a trapezoidal shape TEG and investigated the effect of geometric parameter R_A on device performance ($R_A = A_H/A_L$), where A_H is the cross-sectional area of the top leg end and A_L is that of the bottom leg end). It is found that the design with $R_A = 2$ has reduced thermal stress and improved thermal efficiency. Thus, above two design are selected to compared with the present S-IVCS$_{op}$. For fair comparison, the volumes are kept as 3.96 mm^3 for all the three designs. As shown in Figure 16, the S-IVCS$_{opt}$ design is the optimal one, further demonstrating its advantages. The reason is attributed to the improved temperature profile across the device. Only in S-IVCS$_{opt}$ can the materials operate in their own suitable temperature regime.

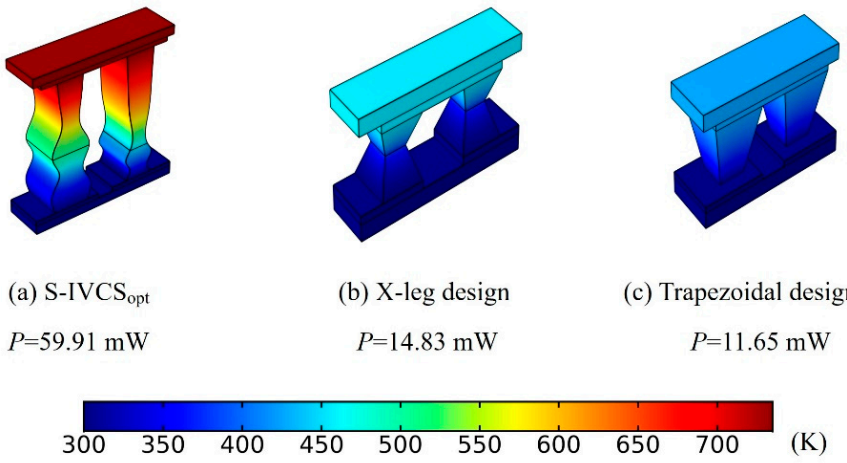

Figure 16. Performance comparison of the proposed design with other studies: (**a**) the present design; (**b**) the X-leg design; (**c**) the trapezoidal design.

It should be indicated that although the performance is significantly improved by the novel S-IVCS design, some limitations also remain. (1) From a fabrication point of view, it is not easy to construct an irregular cross-section by conventional method. However,

with the development of advanced method such as 3D print, the fabrication maybe viable in future. (2) The optimal structure is limited to a specific boundary condition, when the thermal load or cooling temperature are changed, the optimal structure design should be modified. Finding all the optimal structures under different conditions is time-consuming. However, it could be realized by coupling machine learning technology in future.

4. Conclusions

In this work, the feasibility and advantage of a TEG coupled with segmented material and irregularly variable cross-section design was examined. The performance is found to be superior to the already reported structures. The main conclusions and contributions are summarized as follows:

(1) It is demonstrated that neither only segmented design nor only variable cross-section design could reach the optimal performance for a TEG with certain volume. Coupling segmented material and irregularly variable cross-section design together is feasible to further boost the output power.
(2) The optimization results confirm the advantage of the proposed S-IVCS design. Compared with the conventional ones, the output power increased from 39.49 mW to 59.91 mW for the S-IVCS design, and from 38.56 to 41.48 mW for the only variable cross-section design. The betterments were enhanced by 51.71% and 7.57% respectively.
(3) There is complex coupling between the appropriate segmented pattern and the irregularly variable cross-section shape. The optimized topography not only rendered the thermal resistance re-distributed but also altered the electrical resistance profile, leading to improved temperature and potential distribution.
(4) The optimized structure by S-IVCS design strategy reaches a higher average figure of merit than conventional designs. It provides a promising method to enhance TEG performance without an increase in the cost of manufacturing.

Author Contributions: Conceptualization, T.-H.W.; methodology, Y.-Q.Z. and J.S.; software, J.S.; validation, J.S.; formal analysis, Y.-Q.Z., J.S., and G.-X.W.; investigation, J.S. and G.-X.W.; resources, J.S; data curation, Y.-Q.Z., J.S., and G.-X.W.; writing—original draft preparation, T.-H.W.; writing—review and editing, Y.-Q.Z., J.S., G.-X.W., and T.-H.W.; supervision, T.-H.W.; funding acquisition, T.-H.W. All authors have read and agreed to the published version of the manuscript.

Funding: This research was supported by the National Natural Science Foundation of China (Grant No. 51876059) and the Fundamental Research Funds for the Central Universities (Grant No. 2021MS009).

Conflicts of Interest: The authors declare no conflict of interest.

References

1. DiSalvo, F.J. Thermoelectric cooling and power generation. *Science* **1999**, *285*, 703–705. [CrossRef] [PubMed]
2. Bell, L.E. Cooling, heating, generating power, and recovering waste heat with thermoelectric systems. *Science* **2008**, *321*, 1457–1461. [CrossRef] [PubMed]
3. Tohidi, F.; Holagh, S.G.; Chitsaz, A. Thermoelectric Generators: A comprehensive review of characteristics and applications. *Appl. Therm. Eng.* **2022**, *201*, 117793. [CrossRef]
4. Shakouri, A. Recent developments in semiconductor thermoelectric physics and materials. *Annu. Rev. Mater. Res.* **2011**, *41*, 399–431. [CrossRef]
5. Gayner, C.; Kar, K.K. Recent advances in thermoelectric materials. *Prog. Mater. Sci.* **2016**, *83*, 330–382. [CrossRef]
6. Shittu, S.; Li, G.Q.; Zhao, X.D.; Ma, X.L. Review of thermoelectric geometry and structure optimization for performance enhancement. *Appl. Energy* **2020**, *268*, 115075. [CrossRef]
7. Karana, D.R.; Sahoo, R.R. Influence of geometric parameter on the performance of a new asymmetrical and segmented thermoelectric generator. *Energy* **2019**, *179*, 90–99. [CrossRef]
8. Wang, X.J.; Qi, J.; Deng, W.; Li, G.P.; Gao, X.D.; He, L.X.; Zhang, S.X. An optimized design approach concerning thermoelectric generators with frustum-shaped legs based on three-dimensional multiphysics Model. *Energy* **2021**, *233*, 120810. [CrossRef]
9. Maduabuchi, C.; Njoku, H.; Eke, M.; Mgbemene, C.; Lamba, R.; Ibrahim, J.S. Overall performance optimisation of tapered leg geometry based solar thermoelectric generators under isoflux conditions. *J. Power Sources* **2021**, *500*, 229989. [CrossRef]

10. Yin, T.; Li, Z.M.; Peng, P.; Liu, W.; Shao, Y.Y.; He, Z.Z. Performance analysis and design optimization of a compact thermoelectric generator with T-Shaped configuration. *Energy* **2021**, *229*, 120652. [CrossRef]
11. Maduabuchi, C.C.; Eke, M.N.; Mgbemene, C.A. Solar power generation using a two-stage X-leg thermoelectric generator with high-temperature materials. *Int. J. Energy Res.* **2021**, *45*, 13163–13181. [CrossRef]
12. Khalil, A.; Elhassnaoui, A.; Yadir, S.; Abdellatif, O.; Errami, Y.; Sahnoun, S. Performance comparison of TEGs for diverse variable leg geometry with the same leg volume. *Energy* **2021**, *224*, 119967. [CrossRef]
13. Sahin, A.Z.; Yilbas, B.S. The thermoelement as thermoelectric power generator: Effect of leg geometry on the efficiency and power generation. *Energy Convers. Manag.* **2013**, *65*, 26–32. [CrossRef]
14. Wang, P.; Wang, B.; Wang, K.; Gao, R.; Xi, L. An analytical model for performance prediction and optimization of thermoelectric generators with varied leg cross-sections. *Int. J. Heat Mass Transf.* **2021**, *174*, 121292. [CrossRef]
15. Zhang, G.; Fan, L.; Niu, Z.; Jiao, K.; Diao, H.; Du, Q.; Shu, G. A comprehensive design method for segmented thermoelectric Generator. *Energy Convers. Manag.* **2015**, *106*, 510–519. [CrossRef]
16. Chen, W.H.; Chiou, Y.B. Geometry design for maximizing output power of segmented skutterudite thermoelectric generator by evolutionary computation. *Appl. Energy* **2020**, *274*, 115296. [CrossRef]
17. Yin, T.; He, Z.Z. Analytical model-based optimization of the thermoelectric cooler with temperature-dependent materials under different operating conditions. *Appl. Energy* **2021**, *299*, 117340. [CrossRef]
18. Ge, Y.; Liu, Z.; Sun, H.; Liu, W. Optimal design of a segmented thermoelectric generator based on three-dimensional numerical simulation and multi-objective genetic Algorithm. *Energy* **2018**, *147*, 1060–1069. [CrossRef]
19. Zhao, J.; Xu, W.; Kuang, Z.; Long, R.; Liu, Z.; Liu, W. Segmental material design in thermoelectric devices to boost heat-to-electricity performance. *Energy Convers. Manag.* **2021**, *247*, 114754. [CrossRef]
20. Kishore, R.A.; Sanghadasa, M.; Priya, S. Optimization of segmented thermoelectric generator using Taguchi and ANOVA techniques. *Sci. Rep.* **2017**, *7*, 16746. [CrossRef]
21. Ma, X.; Shu, G.; Tian, H.; Xu, W.; Chen, T. Performance assessment of engine exhaust-based segmented thermoelectric generators by length ratio optimization. *Appl. Energy* **2019**, *248*, 614–625. [CrossRef]
22. Jia, X.; Gao, Y. Estimation of thermoelectric and mechanical performances of segmented thermoelectric generators under optimal operating Conditions. *Appl. Therm. Eng.* **2014**, *73*, 335–342. [CrossRef]
23. Tian, H.; Sun, X.; Jia, Q.; Liang, X.; Shu, G.; Wang, X. Comparison and parameter optimization of a segmented thermoelectric generator by using the high temperature exhaust of a diesel engine. *Energy* **2015**, *84*, 121–130. [CrossRef]
24. Heber, L.; Schwab, J.; Knobelspies, T. 3 kW Thermoelectric Generator for Natural Gas-Powered Heavy-Duty Vehicles—Holistic Development, Optimization and Validation. *Energies* **2022**, *15*, 15. [CrossRef]
25. Hadjistassou, C.; Kyriakides, E.; Georgiou, J. Designing high efficiency segmented thermoelectric generators. *Energy Convers. Manag.* **2013**, *66*, 165–172. [CrossRef]
26. Hatanaka, T.; Korenaga, T.; Kondo, N.; Uosaki, K. Search performance improvement for PSO in high dimensional space. In *Particle Swarm Optimization*; InTech: Rijeka, Croatia, 2009; Chapter 15; pp. 249–260. ISBN 978-953-7619-48-0. [CrossRef]
27. Ali, M.; Pant, M.; Abraham, A. Improving differential evolution algorithm by synergizing different improvement mechanisms. *ACM Trans. Auton. Adapt. Syst.* **2012**, *7*, 1–32. [CrossRef]
28. Garmejani, H.A.; Hossainpour, S. Single and multi-objective optimization of a TEG system for optimum power, cost and second law efficiency using genetic algorithm. *Energy Convers. Manag.* **2021**, *228*, 113658. [CrossRef]
29. Zhu, L.; Li, H.; Chen, S.; Tian, X.; Kang, X.; Jiang, X.; Qiu, S. Optimization analysis of a segmented thermoelectric generator based on genetic algorithm. *Renew. Energ.* **2020**, *156*, 710–718. [CrossRef]
30. Coley, D.A. *An Introduction to Genetic Algorithms for Scientists and Engineers*; World Scientific Publishing Co., Pte. Ltd.: Singapore, 1999.
31. Hu, X.; Yamamoto, A.; Ohta, M.; Nishiate, H. Measurement and simulation of thermoelectric efficiency for single leg. *Rev. Sci. Instrum.* **2015**, *86*, 45103. [CrossRef]
32. Hsu, C.T.; Huang, G.Y.; Chu, H.S.; Yu, B.; Yao, D.J. An effective Seebeck coefficient obtained by experimental results of a thermoelectric generator module. *Appl. Energy* **2011**, *88*, 5173–5179. [CrossRef]
33. Shen, L.; Zhang, W.; Liu, G.; Tu, Z.; Lu, Q.; Chen, H.; Huang, Q. Performance enhancement investigation of thermoelectric cooler with segmented configuration. *Appl. Therm. Eng.* **2020**, *168*, 114852. [CrossRef]
34. Niu, Z.Q.; Yu, S.H.; Diao, H.; Li, Q.S.; Jiao, K.; Du, Q.; Tian, H.; Shu, G.Q. Elucidating modeling aspects of thermoelectric generator. *Int. J. Heat Mass Transf.* **2015**, *85*, 12–32. [CrossRef]
35. Ge, Y.; He, K.; Xiao, L.H.; Yuan, W.Z.; Huang, S.M. Geometric optimization for the thermoelectric generator with variable cross-section legs by coupling finite element method and optimization algorithm. *Renew. Energ.* **2022**, *183*, 294–303. [CrossRef]
36. Ibeagwu, O.I. Modelling and comprehensive analysis of TEGs with diverse variable leg geometry. *Energy* **2019**, *180*, 90–106. [CrossRef]
37. Al-Merbati, A.S.; Yilbas, B.S.; Sahin, A.Z. Thermodynamics and thermal stress analysis of thermoelectric power generator: Influence of pin geometry on device performance. *Appl. Therm. Eng.* **2013**, *50*, 683–692. [CrossRef]